# Photothermal depth profilometry of heat-treated hardened 0.15%–0.2% C, 0.6%–0.9% Mn Steels

Yue Liu, Natalie Baddour, and Andreas Mandelis
*Center for Advanced Diffusion Wave Technologies, Department of Mechnical and Industrial Engineering, University of Toronto, 5 King's College Road, Toronto, Ontario, Canada M5S 3G8*

Clare Beingessner
*B&W Heat Treating Ltd., 390 Trillium Drive, Kitchener, Ontario, Canada N2G 4W6*

(Received 16 September 2003; accepted 2 May 2004)

The thermal-diffusivity depth-profilometric properties of hardened AISI 1018 steel samples (0.15%–0.2% C and 0.6%–0.9% Mn) are investigated from experimental data and compared to their microhardness depth profiles. To fully understand the effect of the individual steps of the heat-treating process on the thermal-diffusivity of the steels, the thermal-diffusivity depth profiles are reconstructed using laser infrared photothermal radiometry. The inverted depth profiles are compared to the results of microhardness testing after each step of carbonitriding and quenching. The comparison shows that there is a good to excellent anticorrelation between hardness and thermal-diffusivity profiles for both carbonitrided and quenched samples with 0.02 in. case depth and gradually worsening anticorrelation trends for 0.04 and 0.06 in. case depths. It is concluded that for this particular steel, both carbon diffusion and the complicated carbonitrided microstructure affect the absolute values of the thermal-diffusivity profiles as well as their depth distribution.  [DOI: 10.1063/1.1765868]

## I. INTRODUCTION

Thermophysical depth profilometry is a thermal-wave inverse-problem technique where thermal-diffusivity profiles of a material are reconstructed from experimental surface data. Specifically for steels, since the thermal diffusivity depends, among other things, on their microstructural properties, monitoring this parameter indirectly gives information on changes that take place as a result of surface or bulk modification processes. Laser processing, case hardening, and coating deposition are examples of such processes. In particular, thermophysical depth profilometry, as implemented by laser photothermal means, has shown promise as a nondestructive alternative to existing costly, time-consuming, and destructive techniques to determine metallurgical properties of case-treated steels.

Various independent groups of researchers have studied the by now well-established anticorrelation between thermal diffusivity and microhardness. Jaarinen and Luukkala[1] made the attempt to study the properties of surface hardness of steel in terms of an inverse process and developed a numerical technique based on the solution of the thermal-wave equation using a two-dimensional finite difference grid. Lan *et al.*[2] used a mathematical reconstruction technique[3] to obtain the thermal conductivity depth profile of quenched steel, and found a close anticorrelation between the depth dependent thermal conductivity and conventionally measured Vickers hardness. Munidasa, Funak, and Mandelis [4] applied the thermal harmonic oscillator (THO) (Ref. 5) method on quenched steels and found an anticorrelation between thermal diffusivity and microhardness, which was not, however, exact. Later, Mandelis, Munidasa, and Nicolaides [6] showed that the results from investigated cold-work depth profiles in rail track samples illustrated the potential of photothermal detph profilometry as a nondestructive, noncontact inspection methodology of rail deterioration as a function of length of service in the train transportation field. From this wealth of evidence it is now established that quantitative diffusivity depth profiles obtained for case-hardened steel anticorrelate, at least qualitatively, with destructive microhardness measurements. In general, despite the thermal-wave inverse problem types of reconstructions applied to steels and the anticorrelation trends observed between thermal diffusivity and hardness, no physical interpretation of the depth profile (mostly for quenched steels) has been attempted other than the evidence that the hardness anticorrelates with thermal diffusivity. Fournier *et al.*[7] used a photoreflectance setup as well as a photothermal radiometry (PTR) setup to reconstruct the thermal-diffusivity depth profiles of hardened steel samples. They, too, showed that there was an anticorrelation between hardness and thermal diffusivity. Walther *et al.*[8] used two different experimental methods to determine the relation between the hardness and thermal diffusivity: the common laser flash technique to estimate the thermal diffusivity of a set of fully hardened, homogeneous specimens with different hardness produced by appropriate heat treatments, and lateral scanning photothermal microscopy to estimate the thermal-diffusivity depth profile from localized measurements that was compared with the hardness depth profile obtained by microindentation. Only very recently have attempts been made to offer physical interpretations of photothermally reconstructed hardness depth profiles in processed steels. Nicolaides, Mandelis, and Beingessner [9] sought to understand the mechanism by which the thermal-diffusivity profiles in carburised and hardened AISI 8620 steel arises. The chemical composition of the AISI 8620 steel is 0.18%/0.23% C, 0.7/0.9% Mn, 0.4%/0.7% Ni,

 

TABLE I. AISI-1018 heat-treated steel sample matrix arranged by case depth.

| Case depth | 0.02 in. (0.5 mm) | 0.04 in. (1.0 mm) | 0.06 in. (1.5 mm) |
|---|---|---|---|
| **Roughness thickness** | Sample 1 | Sample 6 | Sample 11 |
| Front 600 grit (~2.5 $\mu$m) polished | Sample 2 | Sample 7 | Sample 12 |
| | Sample 3 | Sample 8 | Sample 13 |
| Back 200 grit (5 $\mu$m) unpolished | Sample 4 | Sample 9 | Sample 14 |
| | Sample 5 | Sample 10 | Sample 15 |
| Hardness and bulk thermal-diffusivity test samples after carbonitriding (sacrificial) | Sample 5 | Sample 10 | Sample 15 |
| 44, 54, 60 grit sand wheel ground (not polished) to yield symmetric front- and back-surface roughness and hardness conditions | Sample a<br>16-front surface<br>17-back surface | sample b<br>18-front surface<br>19-back surface | Sample c<br>20-front surface<br>21-back surface |

0.4%/0.6% Cr and 0.15%/0.25% Mo. It is a popular, low-carbon, low-alloy steel and can produce high core strength and toughness. In the work of Nicolaides, Mandelis, and Beingessner a set of 8620 steel samples were studied after carburizing and then after quenching. These two steps are normally performed sequentially to produce a quenched, hardened steel but were studied independently so that the origins of the thermal-diffusivity profiles could be understood in detail. That study concluded that the depth distribution of the thermal-diffusivity profile is dominated by carbon diffusion during carburization, while the absolute thermal-diffusivity values are dominated by microstructural changes that occur during quenching. The authors also pointed out that the validity of these conclusions for other types of steel is uncertain.

In order to address this issue of the more general validity of the foregoing conclusions, a similar study was performed on AISI 1018 steel (0.15%–0.2% C and 0.6%–0.9% Mn). While 8620 steel is typically carburized and then quenched in the process of case hardening, 1018 steel is typically carbonitrided and then quenched. This is due to the fact that 1018 steel has low hardenability which requires improvement by adding nitrogen as well as carbon.

## II. MATERIAL AND PROCESSES

In order to further the understanding of how various heat treatments of AISI 1018 steel affect its thermal diffusivity, photothermal radiometry was used to monitor the mechanical hardness in a nondestructive fashion. A cylindrical rod of AISI 1018 steel was chosen for two different heat treatments: (i) carbonitriding and (ii) carbonitriding followed by quenching.

### A. Carbonitriding

For the carbonitriding and quenching processes, cylindrical samples 1 in. in diameter and 1 cm thick were cut from the same rod. The surfaces of the samples were ground with a sand wheel containing a mixture of 44, 54, and 60 grits. The samples were grouped into three sets and each set was case hardened to one specific case depth. That is, there was a set of samples at each case depth of 0.02, 0.04, and 0.06 in. Table I gives the matrix of samples and their corresponding treatment. The samples were processed in a surface combustion Super 30 All case furnace, equipped with a top cool chamber for slow cooling processes. A flow panel located beside the furnace controlled the nitrogen and methanol flow. For the carbonitriding process, a base atmosphere consisting of nitrogen and methanol was used. The aim was to produce a nominal carrier gas composition consisting of 40% nitrogen, 40% hydrogen and 20% CO. To this base atmosphere an addition of enriching methane ($CH_4$) and ammonia ($NH_3$) gas was used. The ammonia was present throughout the entire cycle. The furnace was already conditioned (i.e., ammonia and methane and base atmosphere was set) before the samples were introduced. Flow scopes were used to set and control the ammonia and natural gas (methane) flows. The cycling time and temperature for the carbonitrided samples are shown in Table II.

### B. Quenching

Some carbonitrided samples were subsequently subjected to the quenching treatment. Rapid oil quenching after carbonitriding results in a nonequilibrium martensite structure, which is a function of its carbon content. Low carbon martensites are soft while high carbon martensites are very hard. Carbonitrided and quenched samples with the same case depth have the same carbon and nitrogen diffusion profile since the carbon and nitrogen concentrations are set as a function of case depth in the carbonitriding process. Although both carbonitrided and quenched samples have the same carbon and nitrogen diffusion profile, the hardness profile is not the same. This is due to the fact that the hardness is a function of the mechanical properties of the sample, which are related to the microstructure of the material. This structure depends on the carbon and nitrogen diffusion profiles as well as the quenching rate achieved during heat treatment. The correlation that exists between the carbon concentration profile and microhardness is a nonlinear empirical relationship with the main similarity being a high-to-low carbon concentration for a high-to-low microhardness, respectively.

TABLE II. Carbonitriding cycles for various case depths.

| Cycle (case depth) (in.) | Temperature (F) | Time (h: m) |
|---|---|---|
| 0.02 | 1600 | 1:50 |
| 0.04 | 1700 | 3:20 |
| 0.06 | 1700 | 6:45 |

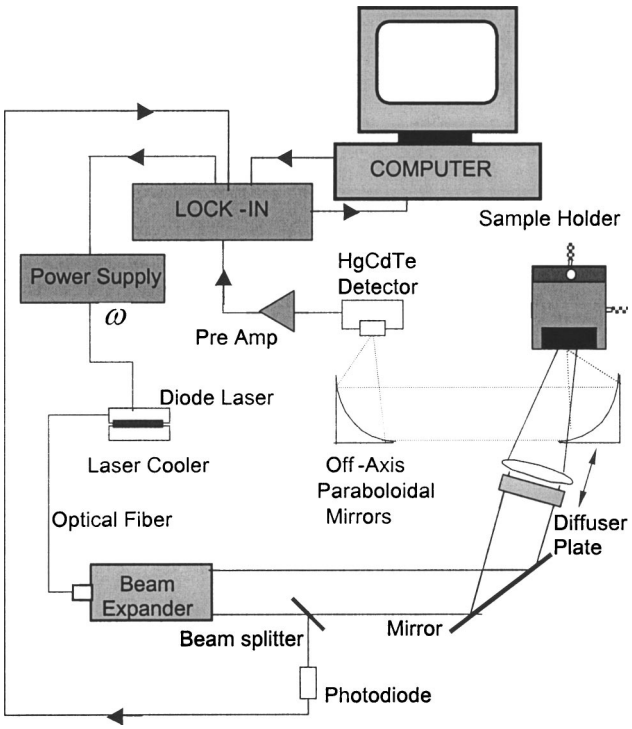


FIG. 1. Photothermal radiometric setup for thermal-diffusivity depth profilometry.

## III. EXPERIMENTAL AND RESULTS

The experimental system for sample frequency scans is shown in Fig. 1. A high power 20-W laser (Jenoptik JOLD-X-CPXL-1L) was current modulated using a Thor Labs high power laser driver with a maximum modulation-frequency capability of 10 kHz and a minimum attainable frequency of 0 Hz (dc). The largely anisotropic multi-mode laser beam was expanded, collimated, and then directed onto the surface of the sample. The infrared (Plauck) radiation from the optically excited sample surface was collected and collimated by two silver-coated, off-axis paraboloidal mirrors and then focused onto a liquid nitrogen cooled HgCdTe (mercury-cadmium-telluride) detector (EG&G Judson Model J15016-M204-S01M-WE-60). The heated area of the sample was at the focal point of the one mirror positioned near the sample and the detector was at the focal point of the other mirror. The HgCdTe detector is a photoconductive element that undergoes a change in resistance proportional to the intensity of the incident infrared radiation. Our detector had an active square-size area of $1\times1$ mm$^2$ and spectral bandwidth of $2-12$ $\mu$m. An antireflection coated germanium window with a transmission bandwidth of $2-14$ $\mu$m was mounted in front of the detector to block any radiation from the laser. Prior to being sent to the digital lock-in amplifier (EG&G Instruments Model 7265), the PTR signal was amplified by a low-noise preamplifier (EG&G Judson PA101), specially designed for operation with the HgCdTe detector. The lock-in amplifier, which was interfaced with a PC, received and demodulated the preamplifier output (thermal-wave amplitude and phase). The process of data acquisition, storage, and frequency scanning was fully automated. A photodiode was used in the optical path to monitor the output power of the laser and correct for fluctuations.

Frequency scans (0.5 Hz–10 kHz) with large laser beam size ($>$1.5 cm) were performed on the carbonitrided 1018 steel samples before and after quenching. The experiments were performed with an expanded beam so that the PTR signals would be in the one-dimensional (depth only) thermal-wave limit and thus simplify the theoretical and computational analysis by avoiding complications due to lateral (radial) heat diffusion. To maintain the one-dimensional heat diffusion formalism assumed in the theory, the laser beam spot size must be made much larger than the maximum profile depth and its intensity spatial profile must be flat. Nearly flat laser spot sizes were achieved by using an optical diffuser in the beam path. System transfer function normalization was achieved by performing the same one-dimensional experiment with a homogeneous (untreated) semi-infinite steel sample of the same type as the treated steels of this study, and using this frequency scan to normalize the frequency scans of the carbonitrided and quenched samples. It was expected that industrial quality samples having the same surface condition and case depth would have similar frequency responses. Under the same processing conditions, however, some of the frequency response curves coincided while other curves diverged from the group, in particular, at high frequencies. Taking into account the fact that the surface roughness was similar for all tested samples, it was hypothesized that the spread of frequency responses might be due to transverse inhomogeneities in some samples following the heat-treating process. To account for possible radial inhomogeneity of any samples, a line scan method was devised to select relatively homogeneous samples among all the experimental samples, as described elsewhere.[10] Transversely inhomogeneous case hardened samples are not suitable candidates for the one-dimensional thermal-diffusivity reconstruction since the theory upon which the algorithm is based assumes that the inhomogeneity is in the depth direction only. The frequency scans of the thus filtered nearly homogeneous samples are shown in Fig. 2.

An independent measurement of the bulk diffusivity of the carbonitrided and quenched samples is required for the numerical inversion of the frequency scans. This is so because the inversion algorithm of the ill-posed thermal-wave inverse problem finds multiple solutions to match the experimental amplitude and phase curves. The only acceptable solution, however, is the one that directs the thermal-diffusivity depth profile to the (measured) bulk value of the sample. To obtain the bulk thermal diffusivity, four thin samples were cut from the rod from which the original samples were obtained. The four thin samples were polished to 600 grit (2.5 $\mu$m) roughness and their thickness was measured. By combining the reflection and transmission methodology described in, Refs. 11 and 12, the bulk thermal diffusivity of steel 1018 was obtained. This methodology involves using the one-dimensional thermal-wave problem, in a single layer of thickness L, in the surface absorption (infinite absorption coefficient) limit. Data self-normalization is implemented by considering the ratio of the signals from the front surface and the back surface. In particular, simple expressions for the

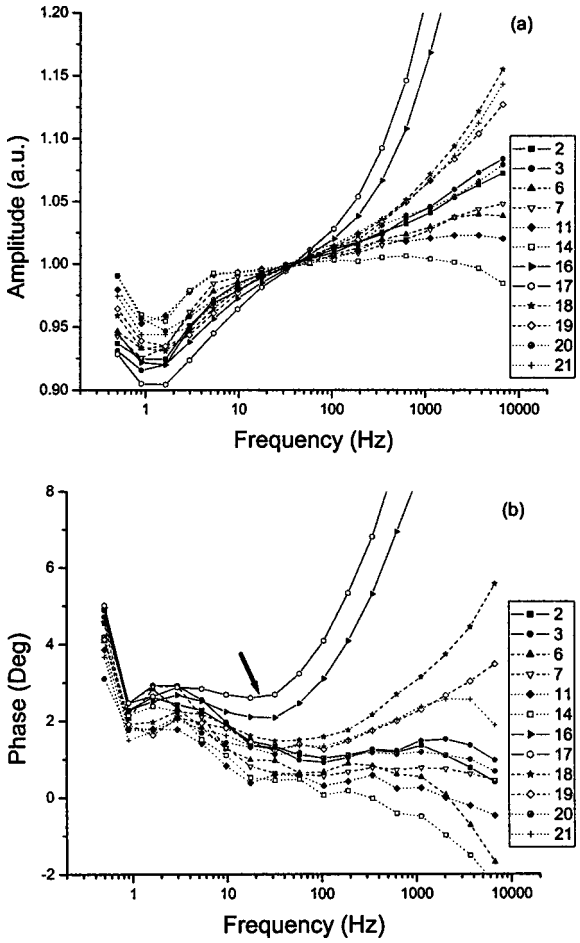


FIG. 2. Normalized and smoothed frequency-scan responses of all selected carbonitrided homogeneous samples (2,3,6,7,11,14,16–21). The arrow shows the cutoff frequency for samples 16 and 17.

difference of the photothermal phase lags between the rear and front configurations can be derived in the low-frequency and high-frequency regions.[12] It can be shown that in the high-frequency (thermally thick) regime, the phase difference between front and rear configurations is given by

$$\Delta\phi = -\left(\sqrt{\frac{\pi}{\alpha}}L\right)\sqrt{f}, \tag{1}$$

where $L$ is the sample thickness, $f$ is the frequency, and $\alpha$ is the thermal diffusivity of the sample. The slope of the $\Delta\Phi$ vs $\sqrt{f}$ curve in the appropriately defined thermally thick frequency range yields the thermal diffusivity $\alpha$ of the material. A similar analysis can be performed in the appropriately defined low-frequency range where it can be shown that the phase difference satisfies

$$\tan(\Delta\Phi) = -\left(\frac{\pi}{\alpha}L^2\right)f. \tag{2}$$

Figure 3 shows an example of the combination of the PTR reflection and transmission experimental results. For the four thin samples used for this measurement, the average diffusivity value from the results obtained by fitting the amplitude curve is 0.144 $cm^2/s$, which is very close to the documented value measured for similar low carbon steels (AISI 1020:0.14 $cm^2/s$).[13]

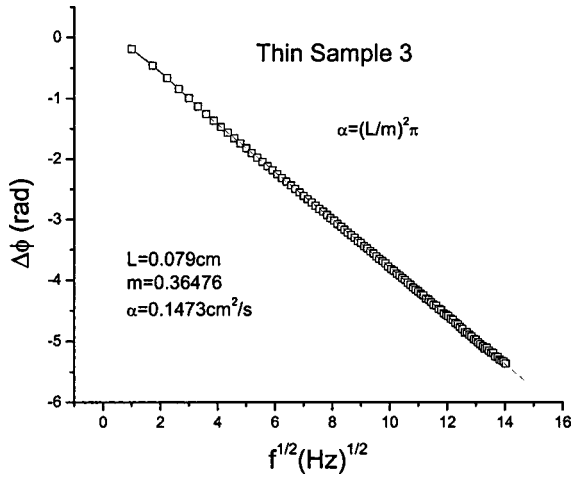


FIG. 3. Combination of thermal-wave reflection-transmission measurements. $L$ represents the thickness of the sample, $m$ represents the slope of the linear fitting to Eq. (1).

## IV. THEORETICAL/NUMERICAL DEPTH-PROFILOMETRIC INVERSIONS

### A. Inversion algorithm

The frequency scans of the carbonitrided and carbonitrided-quenched samples were subjected to an inversion algorithm to produce the thermal-diffusivity depth profiles. The inverse problem methodology has previously been tested in reconstructing the thermal-diffusivity profiles from the experimental data.[4] It was also used to reconstruct thermal-diffusivity depth profiles from case hardened AISI 8620 steels.[9]

To summarize the inversion methodology, the only inhomogeneity is assumed in the depth direction of a laterally infinite solid and a one-dimensional formalism is used. A simple simulated functional dependence of the solid thermal diffusivity is assumed in the form

$$\alpha_s(x) = \alpha_0\left(\frac{1+\Delta e^{-qx}}{1+\Delta}\right)^2, \tag{3}$$

such that $\alpha_s(\infty)=\alpha_\infty$, $\alpha_s(0)=\alpha_0$, and

$$\Delta = \sqrt{\alpha_0/\alpha_\infty} - 1, \tag{4}$$

where $q$ is a constant that determines the rate of thermophysical decay, if $\alpha_0 > \alpha_\infty$, or growth, if $\alpha_0 < \alpha_\infty$.

Using the superposition principle in solving the thermal-wave boundary-value problem and forcing the resultant expression to obey various limiting cases, the surface temperature of a semi-infinite inhomogeneous medium is shown[14] to be

$$T(0,\omega) = \frac{Q_0}{2\sigma_0 k_0}[1 + (R_\infty - 1)\exp(-\sigma_\infty J_\infty)], \tag{5}$$

where

$$J_\infty = \frac{1}{2q}\ln\left(\frac{\alpha_0}{\alpha_\infty}\right), \quad R_\infty = \frac{k_0\sigma_0}{k_\infty\sigma_\infty}. \tag{6}$$

$k_0$ is the thermal conductivity of the surface layer, $Q_0$ is the incident heat flux, and $\sigma_k$ is the complex wave number and is equal to

$$\sigma_k(\omega) = (i+1)\sqrt{\frac{\omega}{2\alpha_k}}. \tag{7}$$

Here $\omega$ represents the angular modulation frequency. The theoretical values of the data pair (amplitude and phase) are calculated by

$$T(0,\omega) = |M(\omega)|e^{i\Delta\phi(\omega)}, \tag{8}$$

where $M(\omega)$ is the thermal-wave amplitude and $\Delta\phi(\omega)$ is the phase at angular frequency $\omega$. At each frequency the amplitude and phase are used to calculate $\alpha_0$ and q of Eq. (1) where $\alpha_\infty$ represents the (assumed) known bulk thermal diffusivity. The actual profile is updated at each frequency by recalculating new parameters of $\alpha_0$ and q. Arbitrary depth profiles may be reconstructed by numerically determining the optimal pair of $\alpha_0$ and q so that the profile sought locally results in the experimentally observed thermal-wave signal amplitude and phase data. Therefore at each $\omega_j$ a system of two equations and two unknowns is solved.

The calculation of the depth parameter $x_j$ is performed based on the fact that as the modulation frequency decreases the thermal-wave probing depth increases. Starting at the highest frequency $\omega_0$, the shortest depth is the shortest thermal length, i.e.,

$$x_0 = \sqrt{\frac{2\alpha_0}{\omega_0}}. \tag{9}$$

The next (lower) frequency $\omega_{j+1}$ corresponds to an increased thermal-wave depth,

$$x_{j+1} = x_j + \sqrt{\frac{2\alpha_{s(j)}}{\omega_{j+1}}} - \sqrt{\frac{2\alpha_{s(j)}}{\omega_j}}, \tag{10}$$

which is then substituted into Eq. (9) to calculate $\alpha_{s(j+1)}$. Once $\alpha_{s(j+1)}$ is calculated the method returns to recursively calculate the increased thermal-wave depth as

$$x_{j+1} = x_j + \sqrt{\frac{2\alpha_{s(j+1)}}{\omega_{j+1}}} - \sqrt{\frac{2\alpha_{s(j)}}{\omega_j}}. \tag{11}$$

Therefore, the depth of each slice depends on $\omega_j$ and $\alpha_{s(j)}$. The true profile is built up by individual slice profiles, with $x_1$ being the first slice corresponding to the highest frequency. The detailed description of the inversion method can be found elsewhere.[14]

### B. Thermal-diffusivity reconstructions and discussion

Before any data inversions could be achieved it was necessary to select only transversely homogeneous samples for reconstruction, as described in Sec. III and Ref. 10, since the theory assumes that the only inhomogeneity is in the depth direction. Furthermore, the high-frequency, largely surface-roughness-related effects required elimination from the frequency scans. Instead of using a mathematical roughness elimination technique[9,15] to obtain thermal-diffusivity depth profiles reconstructed from frequency responses, the high-frequency surface effects were removed from the experimental data by forcing the high-frequency components of the normalized phase and amplitude scans to assume the theoretical values of zero and one, respectively (semi-infinite solid), thus removing that portion of the signal. The "cutoff" frequency for each sample was chosen to be the highest frequency at which the phase achieves a minimum among the several minima. This is done because phase extrema correspond to thermal-wave interference patterns; retaining the extremum can be beneficial for calculating the transport property that generates the thermal wave (thermal diffusivity). Beyond the extremum the shape of the curve can be greatly affected by roughness, an undesirable situation. This choice was made to simplify the roughness removal methodology with regard to the more complete Gaussian roughness elimination method[15] where a Gaussian function is fitted to the high-frequency peaks in the amplitude and phase portions of the signals. This Gaussian is subsequently removed, effectively removing the high-frequency peaks from the signal. In this work, the full high-frequency peaks did not appear within the employed frequency range (10 kHz). Only the onset of the peak was present and thus the Gaussian removal methodology could not be used. However, the frequency at which the phase achieves its highest minimum coincides with the onset of these high-frequency peaks. For this reason it was chosen as the cutoff frequency. As an example, the cutoff frequency for samples 16 and 17 is shown by an arrow in the phase scans of Fig. 2(b).

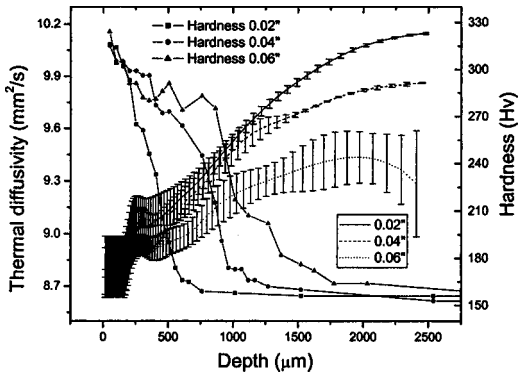


FIG. 4. Thermal diffusivity and hardness as a function of depth for carbonitrided 1018 steel samples 16–21.

The bulk thermal diffusivity of the material is a required input into the inverse problem methodology and the manner in which this was obtained was described in Sec. III. The bulk diffusivity serves as a means of setting the absolute thermal-diffusivity value of the profile and thus reducing the ill conditioning of the problem, thus selecting a unique profile among several possible depth profiles which can yield the same amplitude and phase frequency data. The shape of the profile is primarily determined by the relative change of the experimental data.

The thermal-diffusivity depth profiles reconstructed from the modified frequency responses and the comparison with hardness profiles are shown in Figs. 4 and 5. The error bars

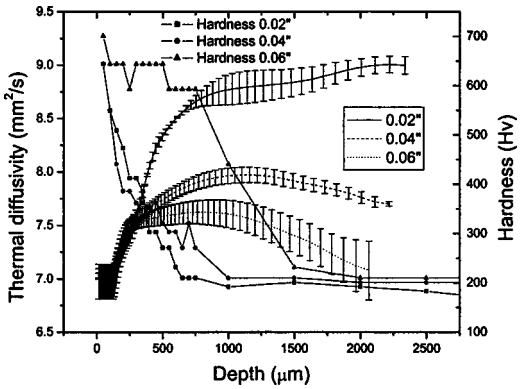


FIG. 5. Thermal diffusivity and hardness as a function of depth for quenched 1018 steel samples 16–21.

represent the standard deviation of the diffusivity depth profiles reconstructed one by one from frequency-scan experimental data from all samples with the same nominal case depth. As the carbonitrided curves show, Fig. 4, the thermal-diffusivity profile is flat at the near-surface area and then increases toward saturation depending on the hardening case depth. The flatness of the thermal-diffusivity curve near the surface region ($<200$ $\mu$m) is artificial and is directly attributed to the fact that the high-frequency portions of the amplitude and phase scans were forced to values of one and zero, respectively, as part of the roughness elimination methodology. The extent of these flat regions (ca. 200 $\mu$m) is indicative of the depth influence of the surface roughness portion on the frequency scans. Compared to the total depth profile of $>2000$ $\mu$m, the effect of this portion on the diffusivity depth profile is essentially negligible. Overall, the curves can be divided into three sections: flat near-surface section, increasing intermediate-depth section, and flat or slightly changing deep-profile section. The intermediate section of increasing diffusivity can be explained by noting that as the distance from the surface increases the hardness decreases. This diffusivity-hardness anticorrelation trend is familiar from other reported thermal diffusivity vs hardness depth profile studies.[1,2,4,7–9,14,15] At depths beyond the diffusion range of the carbon and nitrogen atoms ($\approx$ 500, 1000, and 1500 $\mu$m for each of 0.02, 0.04, and 0.06 in. case depths, respectively), the bulk is intuitively expected to remain unchanged during carbonitriding. As a result, the hardness in this region converges to the same value, and the thermal diffusivity should be expected not to change or change slightly. The reconstructed curves of case depth 0.06 in. further show significant variations between the front-surface and back-surface depth profiles resulting in large error bars; nevertheless, the mean value shows a flat or slightly changing thermal-diffusivity profile. The diffusivity-hardness anticorrelations are not mirror images of each other and exhibit significant variations for the larger case depths. These effects have been observed previously in similar depth-profilometric reconstructions using different kinds of hardened steels.[8,9] Their origin is not necessarily common, but there is evidence[9] that it stems from the role of carbon diffusion and microstructural effects in the hardening process and the influence of those effects on the thermophysical properties of steels.[9] Additional contributing factors may be sought in the inversion algorithm which seeks the (measured independently and assumed known and invariant) bulk thermal-diffusivity value $\alpha_\infty$: It has recently been reported that the bulk microstructure is appreciably affected by the heat treatment,[16] so that the bulk diffusivity of the untreated steel may not be a valid $\alpha_\infty$ value for photothermal reconstructions. This would explain the saturation level dependence of the diffusivity depth profiles in Figs. 4 and 5 on case depth.

Next, even though the PTR phase constancy tests with laser beam size performed in this study guarantee, in principle, the one dimensionality of the thermal-wave inverse problem at beam diameter 1.5 cm, independent calculations of the adequacy of the one-dimensional treatment[16] show that the relation

$$d > 15D \quad (D \text{ — hardness depth}, d \text{ — laser beam diameter})$$

must be obeyed. Even then, it has been observed that compliance with this inequality does not fully eliminate all three-dimensional effects.[16] In the case of Fig. 4 this relation is clearly satisfied only for the 0.02 in. case depth curves. Unfortunately, it was not practical to expand the laser beam much beyond the 1.5 cm diameter limit, as the laser intensity was much compromised resulting in unacceptable photothermal signal-to-noise ratios. Furthermore, given the 1 in. diameter of our samples, it is quite likely that the reconstruction of the deeper diffusivity profiles, especially the 0.06 in. case depth, was somewhat affected by the cylindrical side surfaces of the samples: The built-in assumption of radial infinity in the diffusivity reconstruction theory does not allow for inhibited thermal transfer across the (essentially adiabatic, in agreement with the low air-to-steel thermal effusivity ratio) side surface. The thermal diffusion length of the samples is $\approx$ 3 mm at 0.5 Hz. With a 1.5 cm diameter beam, the 2.1 cm radial thermal-wave extent in comparison with the 2.5 cm (1 in.) diameter of the samples implies that the samples are laterally in the thermally thin regime. The cylindrical side surface, acting as a thermal-wave diffusion barrier, would tend to confine the deeper diffusing thermal-wave field distributions inside the steel thus increasing the mean signal amplitude and decreasing the phase lag at fixed sample radius. In turn, this confinement would result in monotonically decreased effective values of the reconstructed thermal-diffusivity profiles of the thicker case depths, as observed in Fig. 4 (0.04 in. maximum $>$ 0.06 in. maximum).

The diffusivity profiles reconstructed from the quenched samples, Fig. 5, exhibit similar behavior to Fig. 4 and the same general comments apply here as well. Hardness decreases with increasing depth up to a certain value (depending on the hardening case depth), after which the hardness remains constant. Similarly (essentially), flat bulk diffusivity profiles are obtained for the quenched steels, however, again, the best-reconstructed hardness profile through diffusivity is that corresponding to 0.02 in. case depth. The inability of the 0.04 and 0.06 in. diffusivity profiles to reach the level of the 0.02 in. profile, exhibiting monotonically decreasing saturation and local maxima instead, can be tentatively explained

by the variation in bulk thermal diffusivity as a function of case depth heat treating (the treating temperature and time are different for different case depths) and possibly by the breakdown of the assumption of the radial infinite extent of the sample at very low frequencies, leading to lateral thermal-wave confinement. This latter mechanism, also discussed in the foregoing paragraph, would also be consistent with the monotonically increasing downward bending of the flat portion for the 0.04 and the 0.06 in. case depth diffusivity profiles in Fig. 5 (very much like the 0.06 in. case depth in Fig. 4) beyond the $1000-\mu$m range, a feature absent from the 0.02 in. depth profile (and from the 0.04 and 0.02 in. profiles in Fig. 4). With regard to other features of the reconstructed depth profiles, the mechanical hardness for the carbonitrided samples, Fig. 4, saturates at a level about 160 HV whereas the hardness for the quenched samples, Fig. 5, saturates at a level of about 200 HV. This is in keeping with the expectation that the quenched samples are harder than the carbonitrided samples. Similarly, in keeping with the trend of general anticorrelation between diffusivity and hardness, the overall reconstructed thermal diffusivities of the quenched samples are lower than their corresponding values in the carbonitrided sample.

Besides similar experimental evidence of reconstructed thermophysical depth profiles in steels from the photothermal literature,[8,16] physically the diffusivity curve saturation at different values of this parameter for different case depths in our carbonitrided and carbonitrided-quenched samples may primarily be a consequence of the differing carbon and nitrogen contents of the different case depths. In the bulk, both the carbonitrided and quenched samples of the same case depth have the same carbon and nitrogen content. However, the carbonitrided and quenched samples have different microstructures. Microstructure pictures of carbonitrided and quenched samples with 0.02 in. case depth are shown in Fig. 6. Unlike the earlier result of Nicolaides, Mandelis, and Beingessner,[9] both the depth distribution of the thermal-diffusivity profile as well as the absolute values of the thermal diffusivity change when the samples are quenched after carbonitriding. That is to say, the microstructure appears to affect both the absolute values of the thermal-diffusivity profiles as well as depth distribution. To complete the spectrum of possible discrepancy sources between diffusivity and hardness depth profiles, it should be noted[8] that different inversion algorithms will sometimes produce slightly different depth profiles, all with the same overall trend due to the different theoretical assumptions inherent in each method. Such effects, however, cannot account for the large differences between hardness and diffusivity profiles exhibited in Figs. 4 and 5.

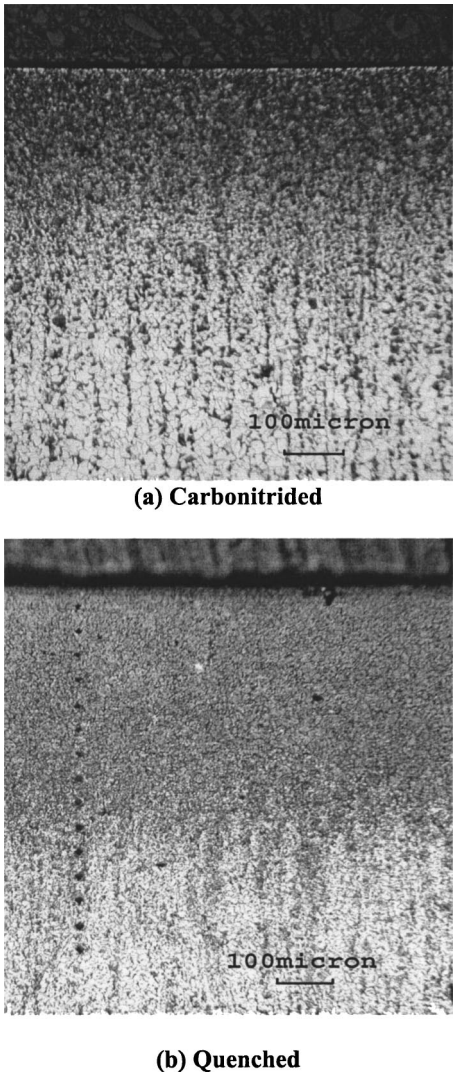


FIG. 6. Cross-sectional microstructure pictures of carbonitrided (a) and quenched (b) samples with 0.02 in. case depth.

## V. CONCLUSIONS

In conclusion, thermal-wave depth profilometry can be used to further the understanding of the effect of heat treating on AISI 1018 steels (0.15%–0.2% C and 0.6%–0.9% Mn) subjected to carbonitriding, and carbonitriding quenching treatments. Comparison of the reconstructed thermal-diffusivity depth profiles of carbonitrided and carbonitrided-quenched samples with the corresponding mechanical hardness depth profiles shows that there is good to excellent anticorrelation between hardness and thermal-diffusivity profiles for both types of heat-treated samples for case depths up to 0.02 in., however, the trends deteriorate for deeper case depths, leading to relationships which are not mirror images. For this particular steel, it appears that both carbon diffusion profiles and the complicated carbonitrided microstructure as well as potential three-dimensional effects due to radial finiteness create dependencies of the bulk values of thermal diffusivity on the heat-treating duration (and thus case depth), which subsequently affect both the absolute values of the thermal-diffusivity profiles as well as depth distribution. Therefore, PTR depth profilometry appears to be a very useful analytical tool in probing this type of case-depth–diffusivity dependencies both in the near-surface regions and in the bulk of heat treated steels with multiple solid-state microstructure phase changes, such as those due to carbonitriding.

## ACKNOWLEDGMENTS

The support of Materials and Manufacturing Ontario (MMO) through an Enabling Contract to A.M. is gratefully

acknowledged. We acknowledge the assistance of Sachin Ghai, B&W Heat Treating Ltd, Kitchener, Ontario, for the heat treating of all the samples, as well as for the hardness measurements on the sacrificial carbonitrided and quenched samples in Table I. We also wish to thank Reza Soltani, Centre for Advanced Coating Technologies, Department of Mechanical and Industrial Engineering, University of Toronto for additional hardness measurements of quenched samples.

[1]J. Jaarinen and M. Luukkala, J. Phys. (Paris) **44**, C6-503 (1983).
[2]T. T. N. Lan, U. Seidel, H. G. Walther, G. Goch, and B. Schmitz, J. Appl. Phys. **78**, 4108 (1995).
[3]T. T. N. Lan, U. Seidel, and H. G. Walther, J. Appl. Phys. **77**, 4739 (1995).
[4]M. Munidasa, F. Funak, and A. Mandelis, J. Appl. Phys. **83**, 3485 (1998).
[5]A. Mandelis, J. Math. Phys. **26**, 2676 (1985).
[6]A. Mandelis, M. Munidasa, and L. Nicolaides, NDT & E Int. **32**, 437 (1999).
[7]D. Fournier, J. P. Roger, A. Bellouati, C. Boue, H. Stamm, and F. Lakestani, Anal. Sci. (Japan Soc. Anal. Chem.) **17**, s158 (2001).
[8]H. G. Walther, D. Fournier, J. C. Krapez, M. Luukkala, B. Schmitz, C. Sibilia, H. Stamm, and J. Thoen, Anal. Sci. **17**, s165 (2001).
[9]L. Nicolaides, A. Mandelis, and C. Beingessner, J. Appl. Phys. **89**, 7879 (2001).
[10]Y. Liu, N. Baddour, and A. Mandelis, J. Appl. Phys. **94**, 5543 (2003).
[11]O. Pessoa, Jr., C. L. Cesar, N. A. Patel, H. Vargas, C. C. Ghizoni, and L. C. M. Miranda, J. Appl. Phys. **59**, 1316 (1986).
[12]A. Balderas and A. Mandelis, Rev. Sci. Instrum. **74**, 5219 (2003).
[13]N. V. Lugueva and S. M. Luguev, Phys. Solid State **44**, 260 (2002).
[14]A. Mandelis, F. Funak and M. Munidasa, J. Appl. Phys. **80**, 5570 (1996).
[15]L. Nicolaides and A. Mandelis, J. Appl. Phys. **90**, 1255 (2001).
[16]H. Stamm, European Community Industrial and Materials Technologies Programme (Brite-Euram) Report No. BE-TN-0522, 2000 (unpublished).